Development 130, 3063-3074

doi:10.1242/dev.00491

DEVELOPMENT AND DISEASE

Conditional inactivation of FGF receptor 2 reveals an essential role for FGF signaling in the regulation of osteoblast function and bone growth

Kai Yu[1], Jingsong Xu[1], Zhonghao Liu[1], Drazen Sosic[2], Jiansu Shao[3], Eric N. Olson[2], Dwight A. Towler[3] and David M. Ornitz[1,*]

[1]Department of Molecular Biology and Pharmacology, [3]Department of Internal Medicine, Washington University Medical School, Campus Box 8103, 660 S. Euclid Avenue, St. Louis, Missouri 63110, USA
[2]Department of Molecular Biology, UT Southwestern Medical Center at Dallas, 5323 Harry Hines Boulevard, Dallas, Texas 75390, USA
*Author for correspondence (e-mail: dornitz@pcg.wustl.edu)

Accepted 3 March 2003

SUMMARY

Human craniosynostosis syndromes, resulting from activating or neomorphic mutations in fibroblast growth factor receptor 2 (FGFR2), underscore an essential role for FGFR2 signaling in skeletal development. Embryos harboring homozygous null mutations in FGFR2 die prior to skeletogenesis. To address the role of FGFR2 in normal bone development, a conditional gene deletion approach was adopted. Homologous introduction of *cre* recombinase into the *Dermo1* (*Twist2*) gene locus resulted in robust expression of CRE in mesenchymal condensations giving rise to both osteoblast and chondrocyte lineages. Inactivation of a floxed *Fgfr2* allele with *Dermo1-cre* resulted in mice with skeletal dwarfism and decreased bone density. Although differentiation of the osteoblast lineage was not disturbed, the proliferation of osteoprogenitors and the anabolic function of mature osteoblasts were severely affected.

Key words: Fibroblast growth factor, FGF, FGF receptor, FGFR2, Endochondral bone growth, Chondrocyte, Osteoblast, Ossification, Dermo1, Twist2, Cre recombinase, Conditional gene deletion

INTRODUCTION

Mutations in fibroblast growth factor receptor (FGFR) 2 are responsible for several clinically distinct craniosynostosis syndromes in humans (Naski and Ornitz, 1998; Ornitz and Marie, 2002; Wilkie, 1997). These syndromes share a common feature; premature fusion of at least one of the cranial sutures. However, craniosynostosis syndromes also have distinct facial features and some have characteristic limb and joint abnormalities and central nervous system dysfunction.

Crouzon syndrome affects suture development and is not associated with limb abnormalities, whereas Pfeiffer syndrome and Jackson-Weiss syndrome are characterized by both craniosynostosis and broad medially displaced toes (Jabs et al., 1994; Rutland et al., 1995). In contrast, Apert syndrome patients develop coronal synostosis, severe bony and soft tissue syndactyly with associated joint fusion, and often have mental retardation (Cohen, 2000). The unique features of craniosynostosis syndromes probably reflect differences in the mechanism by which FGFR activity is altered by specific missense mutations (Wilkie, 1997).

Four FGFR tyrosine kinases bind with varying affinity and specificity to a family of 22 FGF ligands (Ornitz and Itoh, 2001). Ligand binding specificity is regulated by specific sequences in the extracellular region and by the alternative splicing of exons encoding the carboxyl-terminal half of immunoglobulin (Ig) domain III. Alternative splicing of *Fgfr2* is tissue specific, resulting in epithelial variants (b splice forms) and mesenchymal variants (c splice forms) (Miki et al., 1992; Naski and Ornitz, 1998; Orr-Urtreger et al., 1993). Ligand binding studies demonstrate that mesenchymally expressed ligands such as FGF7 and 10, activate FGFR2b, whereas FGF2, 4, 6, 8 and 9 activate FGFR2c (Ornitz and Itoh, 2001; Ornitz et al., 1996).

The majority of missense mutations in FGFR2 result in some ligand-independent dimerization, phosphorylation and constitutive receptor signaling. Interestingly, a single missense mutation which causes Apert syndrome (P252R or S253W in FGFR2) abolishes its ability to discriminate between epithelially and mesenchymally expressed FGF ligands, providing an explanation for the increased severity of Apert syndrome compared to other craniosynostosis syndromes resulting from mutations in FGFR2 (Anderson et al., 1998; Yu et al., 2000; Yu and Ornitz, 2001).

Gain-of-function mutations in FGFR3 result in three related dwarfing chondrodysplasia syndromes; hypochondroplasia,

achondroplasia (ACH) and thanatophoric dysplasia (TD) (Naski and Ornitz, 1998; Ornitz and Marie, 2002). *Fgfr3* is expressed in the cartilage of the developing embryo, prior to formation of ossification centers. In the epiphyseal growth plate, *Fgfr3* is expressed in proliferating and prehypertrophic chondrocytes. Mouse models for ACH and TD demonstrate that activation of FGFR3 inhibits chondrocyte proliferation and differentiation (Chen et al., 1999; Chen et al., 2001; Iwata et al., 2001; Li et al., 1999; Naski et al., 1998; Segev et al., 2000; Wang et al., 1999). In contrast, mice lacking *Fgfr3* exhibit skeletal overgrowth (Colvin et al., 1996). Together, these data establish *Fgfr3* as a negative regulator of endochondral bone growth.

Mice homozygous for null alleles of *Fgfr2* die at embryonic day 10.5 (E10.5) with multiple defects in organogenesis, including the absence of limb buds (Xu et al., 1998). Specific deletion of the b exon of *Fgfr2* results in a neonatal lethal phenotype, also lacking limb buds (De Moerlooze et al., 2000). This phenotype is similar to that of mice lacking *Fgf10* (Min et al., 1998; Sekine et al., 1999). At E10.5, skeletal development has not progressed beyond the condensation stage. However, *Fgfr2* is expressed at high levels in condensed mesenchyme that will give rise to cartilage and bone and later in the perichondrial and periosteal tissues that give rise to osteoblasts (Ornitz and Marie, 2002). To evaluate the function of *Fgfr2* in skeletal development, we used the conditional gene silencing approach to specifically disrupt *Fgfr2* signaling in the chondrocyte and osteoblast lineages. We show that *Fgfr2* is not required for osteoblast differentiation but is essential for osteoblast proliferation and for the maintenance of osteoblast anabolic function.

MATERIALS AND METHODS

Generation of *Dermo1-cre* mice

The *Dermo1* targeting vector (Fig. 1A) was constructed by inserting a 5′ 7 kb *Eco*RI-*Not*I genomic fragment and a 3′ 1.5 kb *Bsp*EI-*Hin*dIII genomic fragment, which flanks exon 1 of *Dermo1*, into *Eco*RI-*Eco*RV, and *Eco*RV-*Hin*dIII sites of pBS-KS, respectively. A *cre* cDNA sequence (Lewandoski et al., 1997b) was cloned into a *Sal*I-*Kpn*I site at the 3′ end of the 5′ arm to generate pBS-7-cre. A FRT2-neo selectable marker, was constructed by inserting a PGK/neo cassette (Tybulewicz et al., 1991) into the *Sna*BI site of pFRT2 (Dymecki, 1996). The FRT-neo fragment was then excised with *Eco*RI and cloned into an *Eco*RI site at the 5′ end of the 3′ arm to generate pBS-1.5-neo. The targeting construct was assembled by cloning the 5′ 7-cre fragment into a 5′ *Not*I site in pBS-1.5-neo. Following linearization, RW4 ES cells were electroporated with the targeting vector and selected with G418. Antibiotic resistant clones were screened by DNA blot analysis of *Xho*I-digested and *Eco*RV-digested genomic DNA using external 5′ and 3′ probes, respectively (Fig. 1A). Primer D1 (5′-AACTTCCTCTCCCGGAGACC) and D2 (5′-CCGGTTATTCAACTTGCACC), which were localized in the intron sequence 5′ of exon 1 of *Dermo1* and in 5′ end of the *cre* sequence, respectively, were used for PCR genotyping of *Dermo1-cre* (370 bp product) (Fig. 1A, Fig. 2D).

Generation of *Fgfr2^{flox}* mice

The 34-bp loxP sequence was introduced into *Fgfr2* genomic sequence with two complementary oligonucleotides, loxP1 5′-CTAGA**GATATC**ATAACTTCGTATAGCATACATTATACGAAGTTATT and loxP2 5′-CTAGAATAACTTCGTATAATGTATGCTATACGAAGTTAT**GATATC**T, which were annealed to form a loxP linker with overhanging *Xba*I ends (underlined). An *Eco*RV site (bold) was placed at the 5′ end of the loxP sequence for further cloning and DNA blot genotyping. A 5.7 kb *Eco*RI-*Hin*dIII genomic fragment, which contained exon 7 (IIIa), exon 8 (IIIb) and exon 9 (IIIc) of *Fgfr2*, was used to generate the 5′-half of the targeting vector by replacing a *Bam*HI site in intron 7 with a *Spe*I site and inserting the loxP linker. A 4.4 kb *Hin*dIII genomic fragment, which contained exon 10 (encoding the transmembrane (TM) domain), was used to generate the 3′-half of the targeting vector by inserting the loxP linker into a *Xba*I site in intron 10 and the FRT-neo cassette into the *Eco*RV site of the loxP linker. RW4 ES cells were transfected and screened by DNA blot analysis of *Eco*RV/*Hin*dIII-digested and *Eco*RV-digested DNA using 5′ and 3′-probes, respectively (Fig. 2A).

To generate the *Fgfr2$^{\Delta}$* allele, *Fgfr2$^{+/flox}$* heterozygous mice were mated with *β-actin-cre* mice (Lewandoski et al., 1997a) and F_1 animals were screened for the presence of *Fgfr2^{flox}* and *β-actin-cre* alleles. The double heterozygous mice were then mated to wild-type mice to obtain a germline-transmitted *Fgfr2$^{\Delta}$* allele.

Primer F1 (5′-ATAGGAGCAACAGGCGG), F2 (5′- TGCAAGAG-GCGACCAGTCAG) and F3 (5′- CATAGCACAGGCCAGGTTG) were used for PCR genotyping of *Fgfr2* alleles. F1 and F2 produced a 142 bp and a 207 bp fragment from wild type and *Fgfr2^{flox}* alleles, respectively, and F1 and F3 produced a 471 bp fragment from the *Fgfr2$^{\Delta}$* allele (Fig. 2D).

Skeletal preparations and radiography

Skeletons were prepared as described previously (Colvin et al., 1996). Radiography studies were carried out using a Specimen Radiography System (Faxitron X-ray Corporation, IL) X-ray source. Bone mineral density was determined using dual energy X-ray absorptiometry (DEXA) with a PIXImus Mouse Densitometer (GE Lunar Medical Systems).

β-galactosidase histochemistry

For whole-mount staining, E11.5 embryos were fixed in 4% paraformaldehyde in PBS for 60 minutes, washed in PBS and stained in β-gal staining buffer (5 mM $K_3Fe(CN)_6$, 5 mM $K_4FE(CN)_6$•$3H_2O$, 1 mM $MgCl_2$, 0.01% sodium desoxycholate, 0.009% NP40, 0.002% X-gal) for 8 hours, at 4°C. After post-fixing in 4% paraformaldehyde, the limb buds were cut off, embedded in paraffin wax and sectioned (4 μm). E15.5 embryos, immediately after dissection were embedded in OCT at –20°C and sectioned (8 μm). Frozen sections were dried at room temperature for 20 minutes, fixed in 4% paraformaldehyde for 10 minutes and stained for 2 hours at 37°C. At postnatal ages, the bones of the mice were dissected, fixed in 4% paraformaldehyde in PBS, decalcified in 14% EDTA for 10 days at 4°C and embedded in OCT at –20°C. 8 μm frozen sections were stained for 2 hours at 37°C. All sections were counter stained with Nuclear Fast Red.

Histological analysis

Tissues were fixed in 4% paraformaldehyde in PBS, decalcified in 14% EDTA and embedded in paraffin wax. Sections were stained with Hematoxylin and Eosin (H&E), von Kossa staining (for minerized bone tissues) or tartrate resistant alkaline phosphatase (TRAP) staining (for osteoclast activity). Computer imaging using AxioVision 3.0 software (Zeiss) was used for histomorphometric analysis. The bone volume and tissue volume were measured on the trabecular bone region of the proximal tibia, including both the primary and secondary spongiosa. The length of proliferating and hypertrophic chondrocyte zones and the length of the metaphysis was measured along the midline of the proximal tibia growth plate.

Osteoblasts and osteoclasts in the primary spongiosa were counted in a region extending 100 μm from the chondro-osseous junction and including the entire width of the metaphysis. The total areas counted were measured using AxioVision 3.0 image software (Zeiss).

The mineral apposition rate (MAR) was determined by calcein double labeling. Mice were injected with calcein (20 mg/kg) 13 days

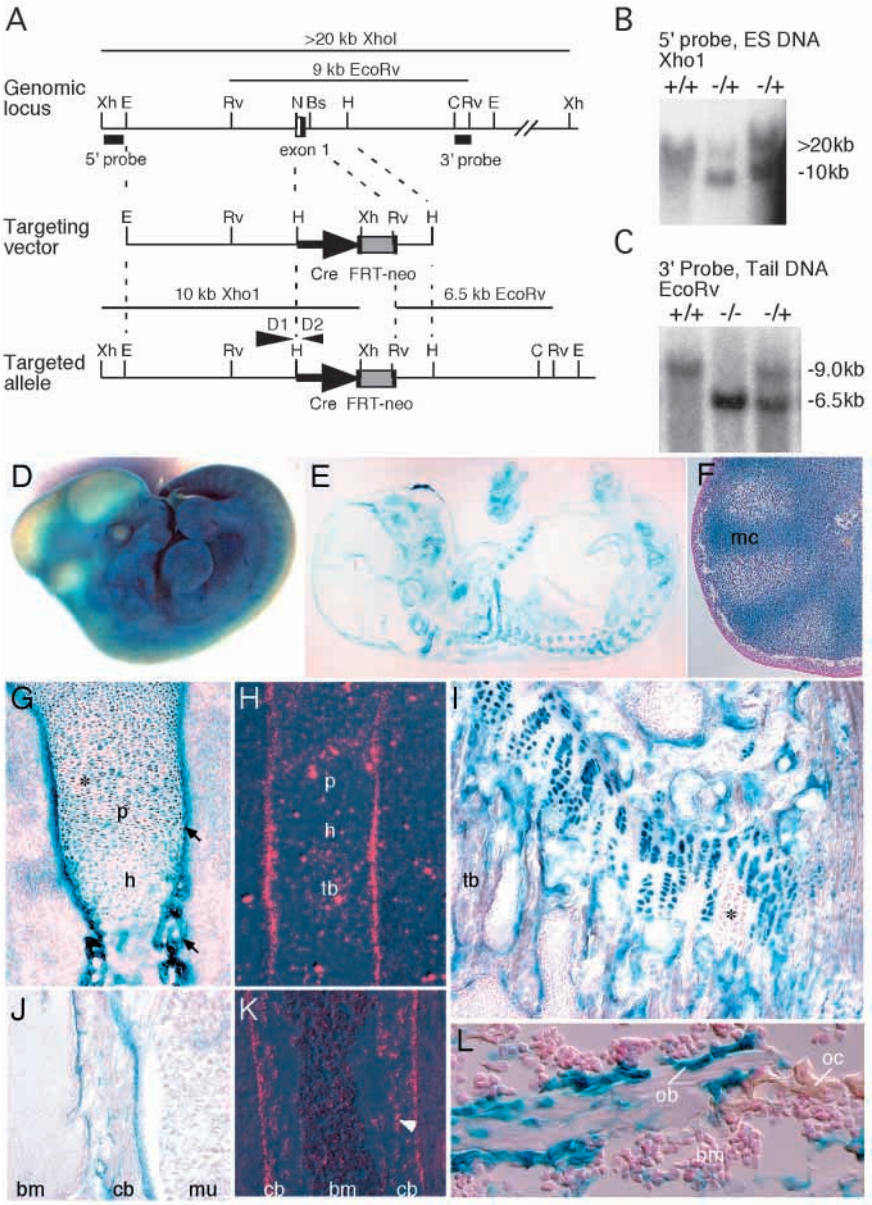

Fig. 1. Generation of *Dermo1-cre* mice and tissue-specific activity of the *Dermo1*-CRE recombinase. (A) A schematic representation of the *Dermo1* genomic locus, the targeting vector and the mutant allele generated following homologous recombination. The arrow represents the *cre* gene and its transcriptional orientation. The length of diagnostic *Xho*I and *Eco*RV genomic restriction fragments are indicated by solid lines. Locations of the probes (5′ and 3′) used for DNA blot analysis and the primers (D1 and D2) used for PCR genotyping are indicated by filled boxes and arrowheads, respectively. FRT-neo contains a PGK-neo cassette (gray bar) flanked by flip recombination sites (black bar). (B) DNA blot analysis of *Xho*I-digested genomic DNA from embryonic stem cells hybridized with the 5′ probe. (C) DNA blot analysis of *Eco*RV-digested tail DNA hybridized with the 3′ probe. (D) Whole-mount detection of β-gal activity in an E11.5 embryo. Note that neural tissue is not stained. (E) Frozen sagittal section of an E15.5 embryo stained for β-gal activity. (F) Paraffin wax section of an E11.5 forelimb bud from the embryo shown in D. Note that the ectodermal epithelium is negative and the mesenchymal condensations (mc) are positive for β-gal activity. (G) Frozen section of an E16.5 femur. The perichondrium and periosteum (arrows) are uniformly stained for β-gal activity. (I,J,L) Frozen section of adult tibia, showing β-gal activity in the growth plate (I), cortical bone (J) and osteoblasts lining bone trabecula (L). Bone marrow and muscle are not stained; F,G,I,J,L are counterstained with Nuclear Fast Red. Note that there are small clusters of unlabeled chondrocytes (*) in the growth plate (G,I). (H,K) In situ hybridization detection of *Fgfr2* expression in developing bone using a probe that detects the tyrosine kinase domain. (H) E16.5 femur. (K) The diaphysis of a P7 femur. Note *Fgfr2* expression in diaphyseal lacunae (arrowhead). Bs, *Bsp*EI; C, *Cla*I; E, *Eco*RI; H, *Hin*dIII; N, *Not*I; Rv, *Eco*RV; Xh, *Xho*I. bm, bone marrow; cb, cortical bone; h, hypertrophic zone; mc, mesenchymal condensation; ob, osteoblast; oc, osteoclast; p, proliferation zone; tb, trabecular bone.

and 4 days prior to sacrifice. Following dissection, long bones were fixed in 70% ethanol and embedded in polymethyl methacrylate resin for sectioning. Coronal sections of comparable anatomic position were examined by fluorecence microscopy. The mean distance between the calcein double labels was measured using AxioVision 3.0 image software (Zeiss).

Analysis of cell proliferation

Anti-BrdU immunohistochemistry was carried out as previously described (Naski et al., 1998). Proliferating osteoblasts were counted as described above for total osteoblasts. The percentage of BrdU-positive nuclei versus total nuclei was calculated as the proliferation index.

RT-PCR

Total RNA was prepared from E10.5 whole embryos or from legs of E16.5 embryos using the RNeasy kit (Qiagen) according to the manufacturer's instructions. At E10.5, the amniotic membrane was removed and $Fgfr2^{\Delta/\Delta}$ embryos were identified by lack of limb buds. At E16.5, legs were dissected from the whole embryos and the skin were carefully removed. First strand cDNA synthesis and subsequent PCR amplification were carried out as described previously (McEwen and Ornitz, 1997). The forward primer 5′-CAAAGGCAACTACACCTGCC and the reverse primer 5′-CAGC-CATGACTACTTGCCCG used in RT-PCR analysis were located in exon 6 and 12 of *Fgfr2*, respectively. qRT-PCR was performed on an Applied Biosystems Gene Amp 5700 Sequence Detection system using Sybr Green fluorescent dye binding to PCR products (Bustin, 2000). Osteocalcin gene expression was quantified as previously described (Willis et al., 2002).

In situ hybridization

In situ hybridization was performed as described previously (Liu et al., 2002). The *Fgfr2* IIIcTM domain probe, which is 348 bp long and includes exon 9 (IIIc) and 10 (TM) sequences, was generated by PCR amplification with forward primer 5′-CCGCCGGTGTTAACACCAC and reverse primer 5′-TGTTACCTGTCTCCGCAG and cloned into the pGEM-T EASY vector (Promaga). Plasmids used for generating ^{33}P-labeled riboprobes were: *Fgfr1* (Peters et al., 1992), *Fgfr2-TK* (De Moerlooze et al., 2000), *collagen type I* (Metsaranta et al., 1991);

osteocalcin (provided by K. Nakashima); *osteopontin* (provided by K. Lee) and *Cbfa1* (*Runx2*; provided by K. Nakashima).

RESULTS

Generation of *Dermo1-cre* mice

Dermo1 is a basic helix-loop-helix transcription factor that is highly expressed in mesodermal tissues during embryogenesis. During skeletal development, *Dermo1* is expressed in condensed mesenchyme and later in perichondrial and periosteal cells surrounding cartilage (Li et al., 1995). Because the transcriptional regulatory elements of *Dermo1* have not been characterized, homologous recombination was used to replace the first exon of *Dermo1* with *cre* recombinase (Fig. 1A). One hundred and thirty ES cell clones were screened and two homologous recombinants were identified (Fig. 1B). Both clones were injected into blastocysts and one germline chimera was obtained (Fig. 1C). Mice heterozygous for the targeted allele (*Dermo1*$^{cre/+}$) were phenotypically normal.

To test in vivo function and tissue specificity of *Dermo1*-CRE, *Dermo1*$^{cre/+}$ mice were mated to *Rosa26* reporter mice (*R26R*) in which the original β-galactosidase (β-gal) insertion into the *Rosa26* locus was disrupted by insertion of a *loxP-neo* cassette (Soriano, 1999). The *lacZ* gene can be reactivated through CRE-mediated excision of the loxP-*neo* sequence (Soriano, 1999). In double heterozygous (*Dermo1*$^{cre/+}$; *R26R*/+) embryos or mice β-gal activity was detected at the surface of the embryo as early as E9.5 and in mesodermal tissues such as branchial arches and somites (Fig. 1D). Little β-gal activity was detected in neural and ectodermal tissues (Fig. 1D,E). During endochondral ossification, β-gal activity was first detected in condensed mesenchyme from which both chondrocytes and osteoblasts are derived (Fig. 1F). Later in development β-gal activity was detected in chondrocytes in growth plate cartilage and in osteoblasts in the perichondrium, periosteum and endosteum (Fig. 1G,I,J,L). Occasionally a clone of chondrocytes was observed that failed to express β-gal activity (Fig. 1G,I). Interestingly, bone marrow cells and osteoclasts were negative for β-gal activity (Fig. 1L). During intramembranous ossification in developing sutures, β-gal activity was present at the osteogenic fronts and in surrounding mesenchymal tissues (data not shown).

In situ hybridization studies were used to compare the pattern of *Fgfr2* expression with that of *Dermo1*-CRE activity. Consistent with published data (Delezoide et al., 1998; Orr-

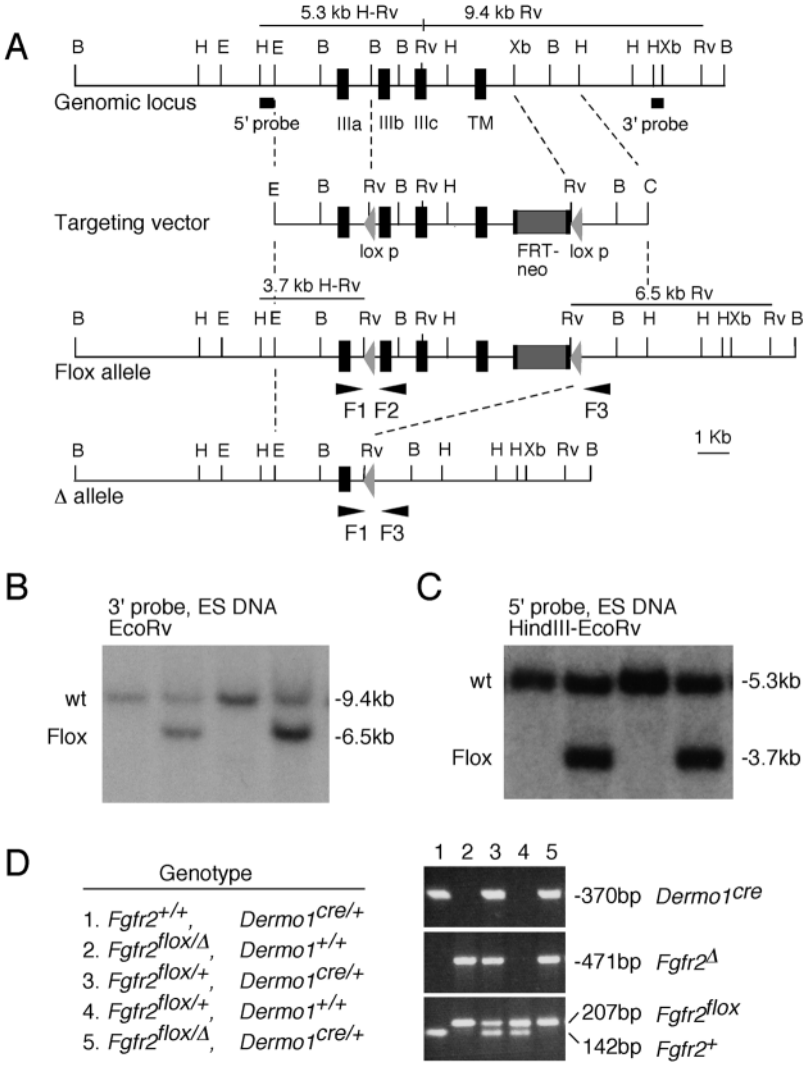

Fig. 2. Generation of a floxed *Fgfr2* allele. (A) Schematic representation of the *Fgfr2* genomic locus, the targeting vector and the *Fgfr2*^{flox} allele following homologous recombination. The loxP sites are indicated by gray arrowheads. The length of diagnostic *Hin*dIII-*Eco*RV and *Eco*RV restriction fragments are indicated by solid lines. The probes (5′ and 3′) used for DNA bolt analysis and the primers (F1, F2 and F3) used for PCR genotyping are indicated by filled boxes and arrowheads, respectively. The Δ allele, generated by CRE-mediated recombination to delete all sequences between the two loxP sites, is shown at the bottom. (B) Southern blot analysis of *Eco*RV-digested genomic DNA from embryonic stem cells hybridized with the 3′ probe. (C) Southern blot analysis of *Hin*dIII-*Eco*RV-digested genomic DNA from embryonic stem cells hybridized with the 5′ probe. (D) PCR analysis of tail DNA (genotype is shown on the left). Primer F1 and F2 distinguish the wild-type (142 bp) and *Fgfr2*^{flox} (207 bp) alleles (bottom panel). Primer F1 and F3 produce a 471 bp fragment from the *Fgfr2*$^{\Delta}$ allele (middle panel). The top panel shows PCR analysis of the *Dermo1*^{cre} allele with primer D1 and D2 using the same DNA samples. A 370 bp fragment is produced from the *Dermo1*^{cre} allele (lanes 1, 3 and 5). Since D2 is localized in the 5′ end of the *cre* sequence, no PCR product is amplified from the wild-type allele (lanes 2 and 4). Note that the 471 bp *Fgfr2*$^{\Delta}$ PCR fragment is amplified from *Fgfr2*$^{+/flox}$; *Dermo-1*$^{cre/+}$ tail DNA (lane 3). This is due to co-expression and deletion of the *Fgfr2*^{flox} allele by *Dermo1*-CRE in tail tissue. B, *Bam*HI; C, *Cla*I; E, *Eco*RI; H, *Hin*dIII; Rv, *Eco*RV; Xb, *Xba*I.

Urtreger et al., 1991; Peters et al., 1992), *Fgfr2* was expressed throughout all phases of skeletal developmental. Initially, *Fgfr2* was expressed in condensing mesenchyme (Delezoide et al., 1998; Orr-Urtreger et al., 1991; Peters et al., 1992). Later in development, *Fgfr2* was predominantly localized to perichondrial and periosteal tissue and weakly to endosteal tissue and trabecular bone (Fig. 1H,K). *Fgfr2* was also present in periarticular chondrocytes but was not detected in growth plate chondrocytes (Fig. 3D,E). In developing sutures, *Fgfr2* expression was found in osteoblasts in the osteogenic fronts (data not shown). The prominent expression of *Fgfr2* in osteoblast lineages suggested an essential function for FGFR2 during skeletal development. Because β-gal activity patterns indicated that osteoblasts were lineage descendants of cells that expressed *Dermo1-cre*, the function of FGFR2 during osteoblast development and bone formation can be studied by a *Dermo1*-CRE-mediated conditional gene silencing approach.

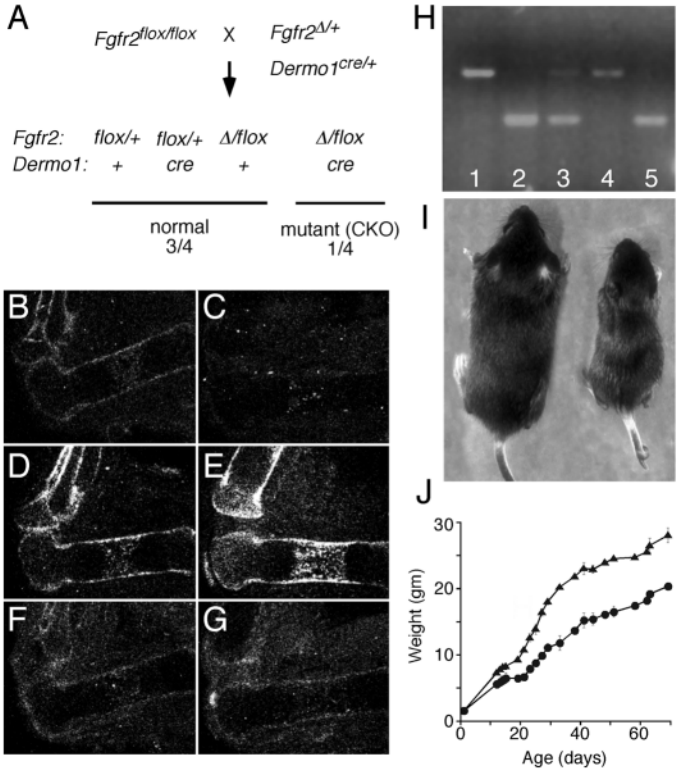

Fig. 3. Generation of *Fgfr2* conditional knockout (*Fgfr2*^{cko}) mice. (A) Mating scheme used to produce *Fgfr2*^{cko} mice (*Fgf2*$^{flox/Δ}$; *Dermo1*$^{cre/+}$). (B-G) In situ hybridization detection of *Fgfr1* and *Fgfr2* in femurs of E16.5 embryos (dark-field images). (B,C), *Fgfr2* expression detected with the transmembrane domain probe, or (D,E) with the tyrosine kinase domain probe. (F,G), *Fgfr1* expression. (B,D,F) Sections from normal control embryos. (C,E,G) Sections from *Fgfr2*^{cko} embryos. (H) RT-PCR analysis of *Fgfr2* expression from wild-type and targeted alleles. Total RNA was prepared from E10.5 whole embryos (lanes 1 and 2) and from leg bones of E16.5 embryos (lane 3-5). Genotype of the embryo in each lane: 1, *Fgfr2*$^{+/+}$; 2, *Fgfr2*$^{Δ/Δ}$; 3, *Fgfr2*$^{Δ/flox}$; 4, *Fgfr2*$^{+/flox}$ and 5, *Fgfr2*$^{Δ/flox}$; *Dermo1*$^{cre/+}$. A 820 bp fragment is generated from *Fgfr2* transcripts of both wild-type and *Fgfr2*^{flox} alleles (lanes 1, 3 and 4) while a 473 bp fragment is generated from the *Fgfr2*^{Δ} allele (lanes 2, 3 and 5). Note that both *Fgfr2* alleles are transcribed in *Fgfr2*$^{Δ/flox}$ mice (lane 3) and full-length *Fgfr2* transcripts are undetectable in skeletal tissues of *Fgfr2*^{cko} mice (lane 5). (I) The appearance of *Fgfr2*^{cko} (right) and control mice (left) at 2 weeks of age. (J) Growth curves of control (triangle) and *Fgfr2*^{cko} (circle) mice.

Construction of *Fgfr2*^{flox} mice

To generate a floxed (flanked by loxP sites) allele of *Fgfr2* that could be inactivated by CRE-mediated recombination, a conditional targeting vector was constructed (Fig. 2A). A 5′ loxP site was inserted in the intron between exon 7 (IIIa) and 8 (IIIb), and a 3′ loxP site was inserted in the intron downstream of exon 10 (TM). An FRT-neo cassette was cloned just upstream of the 3′ loxP site. This design flanked *Fgfr2* sequences encoding the alternatively spliced Ig domain IIIb, IIIc and TM domain encoding exons with loxP sites. Of 343 ES cell clones screened for homologous recombination, 28 3′ end homologous recombinants were identified (Fig. 2B). On screening for the presence of the distal 5′ loxP site, 4 of 28 clones were correctly targeted and also contained the 5′ loxP site (Fig. 2C). These 4 clones were injected into blastocysts and two transmitted the targeted allele into the germline.

Mice heterozygous for the *Fgfr2-flox* allele (*Fgfr2*$^{+/flox}$) were bred to *β-actin-cre* transgenic mice (Lewandoski et al., 1997a) to create a germline null allele of *Fgfr2* (*Fgfr2*^{Δ}) (Fig. 2A). The consequence of different allelic combinations of wild type *Fgfr2(Fgfr2*$^{+}$*)*, *Fgfr2*^{flox} and *Fgfr2*^{Δ} alleles showed that all allelic combinations (*Fgfr2*$^{+/flox}$, *Fgfr2*$^{flox/flox}$, *Fgfr2*$^{+/Δ}$ or *Fgfr2*$^{flox/Δ}$) were phenotypically wild type, except for the *Fgfr2*$^{Δ/Δ}$ embryos, which died between E10 and E11. *Fgfr2*$^{Δ/Δ}$ embryos developed no limb buds, and failed to form a functional placenta, a probable cause of early embryonic lethality (data not shown). These phenotypes were consistent with that of other *Fgfr2* null mice (Xu et al., 1998), suggesting that the two inserted loxP sites used for conditional targeting of *Fgfr2* are functional and that the *Fgfr2*^{Δ} allele is a null allele.

The level of *Fgfr2* transcription in E10.5 wild type and *Fgfr2*$^{Δ/Δ}$ embryos was evaluated by semi-quantitative RT-PCR using primers in exons flanking the three targeted exons (Fig. 3H). Similar amounts of mRNA were transcribed from both wild type *Fgfr2* and *Fgfr2*^{Δ} alleles, suggesting that deletion of exons 8-10 did not affect mRNA transcription, processing, or stability. However, proteins translated from the *Fgfr2*^{Δ} transcript, if any, would be non-functional because of the lack of exons required for ligand binding (IIIb or IIIc) and membrane insertion (TM domain).

Generation of *Fgfr2* conditional knockout (CKO) mice

To conditionally inactivate *Fgfr2* in the developing skeleton, *Fgfr2*$^{+/Δ}$*; Dermo1*$^{cre/+}$ double heterozygous mice were mated with *Fgfr2*$^{flox/flox}$ homozygous mice (Fig. 2D, Fig. 3A). *Fgfr2* conditional knockout (*Fgfr2*^{cko}) mice (*Fgfr2*$^{flox/Δ}$*; Dermo-1*$^{cre/+}$) were born alive with the expected Mendelian frequency (~25%). The efficiency of *Dermo1*-CRE-mediated recombination was assessed by detecting *Fgfr2* expression in developing long bones of control and *Fgfr2*^{cko} mice by in situ hybridization (Fig. 3B-E) and by RT-PCR (Fig. 3H). An in situ hybridization probe, derived from exons 9 and 10 (encoding IIIc and TM domain, respectively), only detected intact *Fgfr2* in normal control but not *Fgfr2*^{cko} femurs of E16.5 and P10 mice (Fig. 3B,C, and data not shown). In contrast, a probe derived from the tyrosine kinase domains of *Fgfr2* detected

both intact and deleted *Fgfr2*. The probe showed similar expression patterns in both *Fgfr2^{cko}* and control femurs of E16.5 and P10 mice (Fig. 3D,E, and data not shown). RT-PCR analysis also revealed that intact *Fgfr2* transcripts were undetectable in skeletal tissues dissected from *Fgfr2^{cko}* mice (Fig. 3H). Together, these data demonstrated that the *Fgfr2^{flox}* allele was effectively targeted by *Dermo1*-CRE-mediated recombination in developing skeletal tissues. In most experiments an *Fgfr2$^{\Delta}$* allele was incorporated to increase the efficiency of CRE-mediated recombination. However, *Fgfr2$^{flox/flox}$*, *Dermo1$^{cre/+}$* mice appeared phenotypically identical to *Fgfr2$^{flox/\Delta}$; Dermo-1$^{cre/+}$* mice.

FGFR1 is another member of the FGF receptor family that closely resembles FGFR2 in both structure and function. *Fgfr1* could be partially redundant with *Fgfr2* and could be upregulated in mice lacking a functional *Fgfr2* allele. *Fgfr1* expression was therefore examined. The results showed that *Fgfr1* expression clearly overlapped with that of *Fgfr2* in developing bone. However, no difference in *Fgfr1* expression between *Fgfr2^{cko}* and control mice was observed (Fig. 3F,G).

Fgfr2^{cko} embryos and newborn pups were phenotypically similar to littermate controls. However, during early postnatal development, *Fgfr2^{cko}* pups exhibited severe growth retardation and by four weeks of age, *Fgfr2^{cko}* mice were 40-50% smaller than controls (Fig. 3I,J). After a characteristic plateau in growth between 14 and 22 days, *Fgfr2^{cko}* mice showed a relatively normal growth curve. However, adult *Fgfr2^{cko}* mice remained 30-40% smaller than controls. *Fgfr2^{cko}* mice were fertile and had a similar life span to that of controls (>1year).

Skeletal abnormalities in *Fgfr2^{cko}* mice

All *Fgfr2^{cko}* mice exhibited a dwarfism phenotype. At P15 and P21, the femur length of *Fgfr2^{cko}* mice was 87% and 79% of control (Table 1), respectively. Skeletal preparations showed a shortened axial and appendicular skeleton (in 21 of 23 skeletons examined) as well as a domed-shaped skull (Fig. 4A,B). Other skeletal abnormalities were also found in *Fgfr2^{cko}* mice with variable severity. The midline sutures (sagittal and metopic) remained patent and the occipital arch was open at the dorsal midline (in 5 of 7 mice examined) (data not shown). Vertebrae also showed abnormalities, including a non-ossified gap in the dorsal midline of both cervical and thoracic vertebrae and absence of the spinous processes (in 7 of 7 mice examined) (Fig. 4C,D). In *Fgfr2^{cko}* mice, several tarsal joints failed to develop (13 of 13 mice examined) (Fig. 4E-H). The origin of the joint fusion appeared to be a failure of cavitation of the cartilaginous anlage prior to ossification of these bones (Fig. 4E,F).

Table 1. Femur length

Age	*n**	Mean body weight (gm)	Genotype	Mean length (mm)	Length % control	*P* value‡
P15	3	8.4±2.5	Control†	9.68±0.63		
	3	5.4±0.4	*Fgfr2^{cko}*	8.47±0.61	87.50	0.07
P21	5	10.4±1.2	Control†	11.35±0.5		
	5	4.8±0.5	*Fgfr2^{cko}*	8.94±0.4	78.77	<0.001

*One femur per individual animal was examined by X-ray; P15, all female; P21, 2 females, 3 males.

†Genotypes are *Fgfr2$^{+/flox}$; Dermo1$^{cre/+}$, Fgfr2$^{+/flox}$; Dermo1$^{+/+}$* or *Fgfr2$^{flox/\Delta}$; Dermo1$^{+/+}$*.

‡Two-tail *P* value from two-sample *t*-test assuming equal variances.

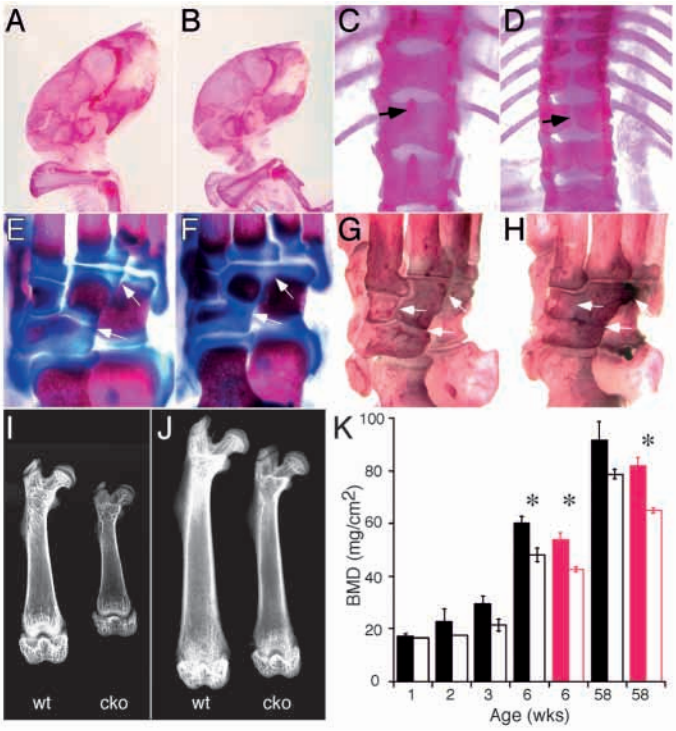

Fig. 4. Skeletal abnormalities and decreased bone density in *Fgfr2^{cko}* mice. (A,B) Alizarin Red stained skulls from P30 control (A) and *Fgfr2^{cko}* (B) mice, showing a dome-shaped skull in the *Fgfr2^{cko}* mouse. (C,D) Dorsal view of the Alizarin Red-stained axial skeleton from a P30 control (C) and *Fgfr2^{cko}* (D) mouse, showing a non-ossified gap in the midline of the vertebrae and the absence of the spinous process (arrows) in the *Fgfr2^{cko}* mouse. (E,F) Alizarin Red- and Alcian Blue-stained tarsal bones from a P7 control (E) and *Fgfr2^{cko}* (F) mouse. All of 13 mice examined showed tarsal bone fusion (arrows). (G,H) Alizarin Red stained tarsal bones from a P60 control (G) and *Fgfr2^{cko}* (H) mouse. The cuneiforme 3 bone is fused with naviculare and cuboideum (arrows) in the *Fgfr2^{cko}* mice. Note that in the adult, the cuneiforme 2 and 3 bones are also fused in the *Fgfr2^{cko}* mice (arrows). (I,J) Radiological analysis of bones from *Fgfr2^{cko}* mice and normal littermates showing decreased bone length and increased radiolucency in *Fgfr2^{cko}* mice. (I) Femurs, P22; (J) femurs, P43; (K) quantitative analysis of bone mineral density by DEXA of femur (black) and lumbar vertebra (red) of mice age 1-58 weeks. Solid bars, control mice; open bars, *Fgfr2^{cko}* mice. *P<0.05.

Reduced bone density in *Fgfr2^{cko}* mice

In addition to the decreased size of the appendicular skeleton, bone mineral density (BMD) was reduced in all *Fgfr2^{cko}* mice examined. Radiographic analysis showed that *Fgfr2^{cko}* mice had decreased BMD compared with age-matched control mice (Fig. 4I,J). Quantitative assessment of the femur and lumbar vertebra by DEXA showed that beginning at 3 weeks of age *Fgfr2^{cko}* mice had significantly decreased BMD. Bone density of *Fgfr2^{cko}* mice increased with age, but always remained lower than that of age-matched control mice even in 58 week-old mice (Fig. 4K).

Fgfr2 is not necessary for differentiation of the osteoblast lineage

Because the osteoblast is the only cell type that engages in bone formation and was one of the cell types effectively targeted by *Dermo1*-CRE, reduced bone density in *Fgfr2*^{cko} mice was likely the result of decreased bone formation as a consequence of osteoblast malfunction. Previous in vitro studies suggested that FGFR signaling affects osteoblast differentiation by regulating osteoblast-specific gene expression (Chikazu et al., 2001; Newberry et al., 1996; Newberry et al., 1997; Zhou et al., 2000). Reduced bone formation in *Fgfr2*^{cko} mice could result from down-regulation of genes required for osteoblast differentiation. The expression of several osteoblast marker genes were examined by in situ hybridization and quantitative RT-PCR (qRT-PCR). At E16.5, although functional *Fgfr2* transcripts were no longer present, skeletal development was not dramatically affected. Skeletal preparations at this age show no evidence of delayed ossification (data not shown) and long bones were of normal size with a well developed and ossified bone collar (Fig. 5A,D). The expression of the genes *Cbfa1*, *osteopontin* and *osteocalcin* showed a similar pattern and intensity in *Fgfr2*^{cko} and control mice (Fig. 5B,C,E,F and data not shown). However, during early postnatal development, histological analysis showed dramatic differences between *Fgfr2*^{cko} mice and normal controls in osteogenic regions (see below). At P7, expression of *Cbfa1*, *collagen type I*, *osteopontin* and *osteocalcin* in *Fgfr2*^{cko} mice showed decreased signal intensity and area, when compared with that of controls (Fig. 5G-L). This corresponded with reduced total osteoblast number in osteogenic regions of *Fgfr2*^{cko} mice (see below). qRT-PCR showed a modest decrease in *osteocalcin* expression in *Fgfr2*^{cko} mice (80% of control, $P<0.05$). *osteopontin* expression was not significantly different in *Fgfr2*^{cko} mice and control mice. These data suggest that loss of *Fgfr2* does not block osteoblast differentiation.

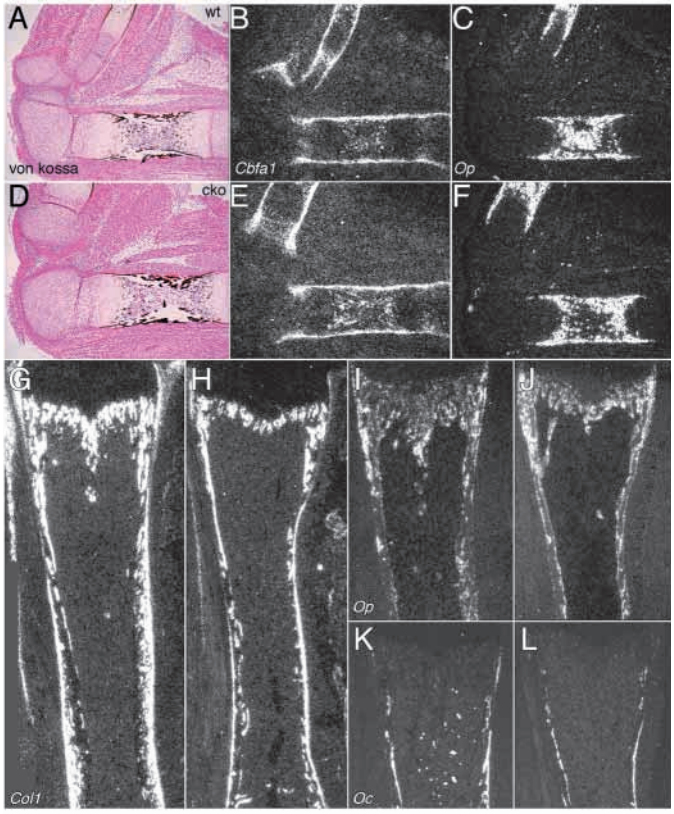

Fig. 5. In situ hybridization detection of osteoblast marker expression in femurs at E16.5 and P7. (A,D) Bright-field images, von Kossa stain. (B,C,E,F,G-L) Dark-field images. (B,E) *Cbfa1* expression at E16.5. (C,F) *osteopontin* expression at E16.5. (G,H) *collagen type I* expression at P7. (I,J) *osteopontin* expression at P7. (K,L) *osteocalcin* expression at P7. (A,B,C,G,I,K) Sections from a control littermate. (D,E,F,H,J,L) Sections from a *Fgfr2*^{cko} mouse.

Defective osteogenesis in postnatal *Fgfr2*^{cko} mice

At embryonic stages, the major osteogenic region is located in the perichondrium and periosteum, which form the bone collar. Vascular invasion of hypertrophic chondrocytes from the central bone collar allows formation of the metaphysis adjacent to the hypertrophic chondrocyte zone (Karsenty and Wagner, 2002; Ornitz and Marie, 2002). The metaphysis contains a large number of active osteoblasts, arranged along calcified spicules of cartilage (Caplan and Pechak, 1987). These cells progressively lay down bone matrix and longitudinally extend trabecular bone. Histologically, osteoblasts that are actively engaged in depositing bone matrix protein appear as plump cuboidal cells with a homogenous basophilic cytoplasm. At the periphery of the metaphysis, multiple longitudinally extended trabeculae merge with perichondrial tissue to form new diaphyseal cortical bone.

In *Fgfr2*^{cko} mice, the metaphysis contained significantly less trabecular bone and in some instances was nearly devoid of trabecular bone (Fig. 6A,B, Table 2 and data not shown). Morphometric analysis showed that trabecular zone length and width was reduced, resulting in a 40% decrease in metaphyseal area (Table 2). Because osteoblasts were distributed throughout the entire metaphysis, the total osteoblast number was reduced. However, osteoblast cell density was not significantly different in the primary spongiosa in *Fgfr2*^{cko} mice (Table 3). Significantly, in *Fgfr2*^{cko} mice, metaphyseal osteoblasts were disorganized along the trabecular surface and showed an atrophic morphology with a granular-appearing cytoplasm (Fig. 6C,D).

Perichondrial and periosteal tissue was also severely affected in *Fgfr2*^{cko} mice. The perichondrium (contiguous with the periosteum) lies adjacent to the growth plate. This multi-layered fibrous collagenous structure consists of a mineralized bone collar, an osteoprogenitor cell layer and an outermost fibroblast-like cell layer (Fig. 6E). Perichondrial/periosteal thickness in *Fgfr2*^{cko} mice was reduced by approximately 50% in regions adjacent to the growth plate and the metaphysis (Fig. 6F). Additionally, the osteoprogenitor cell layer was more compact and contained fewer and atrophic-appearing cells.

The periosteal surface in the mid-diaphysis is another osteogenic zone in developing long bone (Caplan and Pechak, 1987). In control mice, active osteoblasts line the periosteal surface of cortical bone. In *Fgfr2*^{cko} mice, the number of active osteoblasts residing in the diaphyseal periosteum was decreased (Fig. 6G,H). Additionally, in control mice the mid-diaphysis of the femur contained many lacunae, which were occupied by osteoblasts. However, in *Fgfr2*^{cko} mice, the mid-

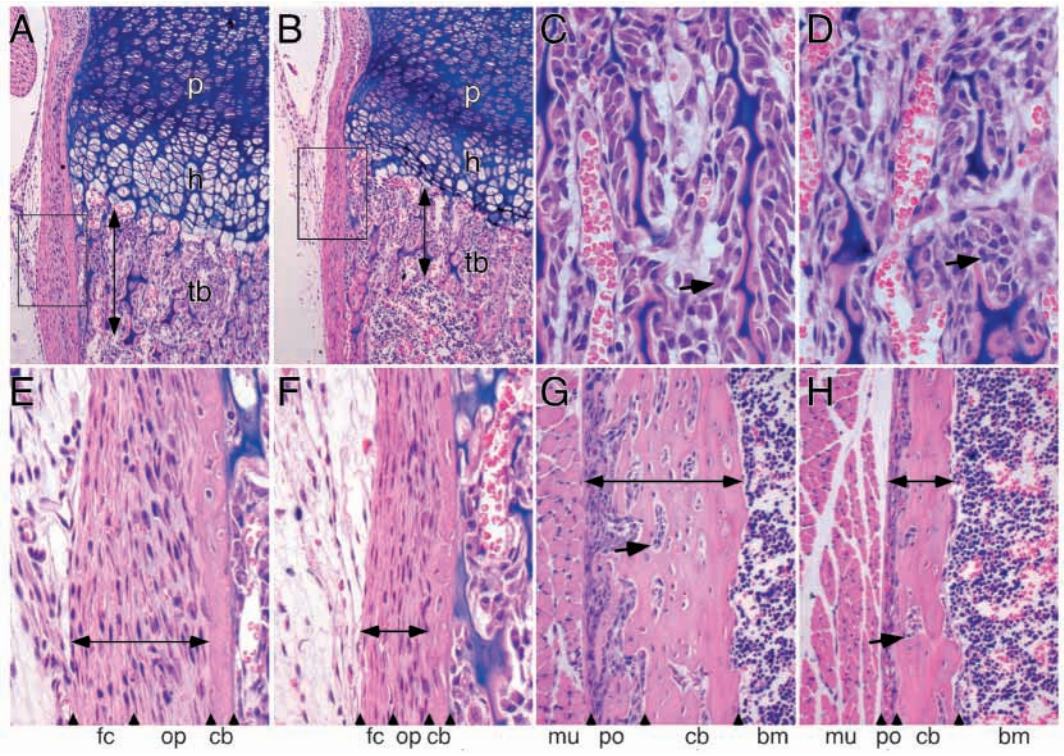

Fig. 6. Defective osteogenesis in *Fgfr2*^{cko} mice. (A,B) H&E stained sections of the distal tibia of P7 mice, showing the epiphyseal growth plate. The length of the metaphysis is indicated by the double-headed arrows. (C,D) Enlarged views showing the morphology of metaphyseal osteoblasts in the proximal tibia. Note that osteoblasts are plump cuboidal cells in the wild-type mouse and become atrophic and irregular in the *Fgfr2*^{cko} mouse (arrows). (E,F) Enlarged view of the boxed regions in A and B showing the morphology of the perichondrium. The thickness of the perichondrium is indicated by double-headed arrows. (G,H) H&E stained sections showing the femoral diaphysis of P7 mice. The thickness of the cortical bone plus the periosteum is indicated by double-headed arrows. Diaphyseal lacunae occupied by active osteoblasts are indicated by arrows. (A,C,E,G) Sections from control littermates. (B,D,F,H) Sections from the *Fgfr2*^{cko} mice. Objective magnification, (A,B) 10×; (C-F) 40×; (G,H) 20×. bm, bone marrow; cb, cortical bone; fc, fibroblast-like cell layer; h, hypertrophic zone; mu, muscle; op, osteoprogenitor layer; p; proliferation zone, po, periosteum; tb, trabecular bone.

Table 2. Bone morphometric data

Genotype	*n**	Mean body weight (gm)	Trabecular zone (μm)	Hypertrophic zone (μm)	Proliferation zone (μm)	Growth plate width (μm)	BV/TV§ (%)
Control†	6	5.1±1.2	415±41	326±34	252±18	1098±87	17.1±1.5
Fgfr2^{cko}	6	3.2±0.5	270±31	223±18	243±16	1009±93	10.2±1.8
% control		63	65	68	96	93	62
P value‡		0.002	<0.0001	<0.0001	0.227	0.04	<0.0001

*Number of animals examined at postnatal day 7.
†Genotypes are *Fgfr2*$^{+/flox}$*; Dermo1*$^{cre/+}$, *Fgfr2*$^{+/flox}$*; Dermo1*$^{+/+}$ or *Fgfr2*$^{flox/\Delta}$*; Dermo1*$^{+/+}$.
‡Two-tail *P* value from two-sample *t*-test assuming equal variance.
§Bone volume/tissue volume.

Table 3. Cell proliferation

Age	*n**	Body weight (gm)	Genotype	Osteoblasts (/0.01mm^2)	% control	*P* value‡	BrdU+ (/0.01mm^2)	Labeling index (%)	% control	*P* value‡
P7	5	4.2	Control†	31.9±2.2			7.9±1.3	24.7		
	5	2.9	*Fgfr2*^{cko}	31.0±1.7	97	0.4	6.3±0.6	20.2	82	0.035
P15	4	8.7	Control†	22.8±3.3			5.6±0.6	24.4		
	4	4.1	*Fgfr2*^{cko}	19.4±3.7	85	0.2	3.6±0.4	18.5	76	0.0014
P25	4	18.8	Control†	13.8±2.4			3.7±0.5	26.5		
	4	9.7	*Fgfr2*^{cko}	14.7±1.3	106	0.6	2.0±0.3	13.4	50	0.0011

*Number of slides counted from one animal.
†Controls; P7 and P15, *Fgfr2*$^{+/flox}$*; Dermo1*$^{cre/+}$; P25, *Fgfr2*$^{+/flox}$*; Dermo1*$^{+/+}$.
‡Two-tail *P* value from two-sample *t*-test assuming equal variances.

diaphyseal region of the femur contained only a few lacunae. The lacunae that were present were more compact and contained fewer atrophic-appearing osteoblasts (Fig. 6H).

The ability of osteoblast to produce bone matrix was assessed by measuring MAR by calcein double labeling. During the third and forth postnatal week the MAR on *Fgfr2*^{cko} mice was too low to measure while control mice had a MAR value of 2.11±0.03 μm/day on the diaphyseal endosteum and 2.43±0.07 μm/day on the diaphyseal periosteum of the femur (Fig. 7A,B).

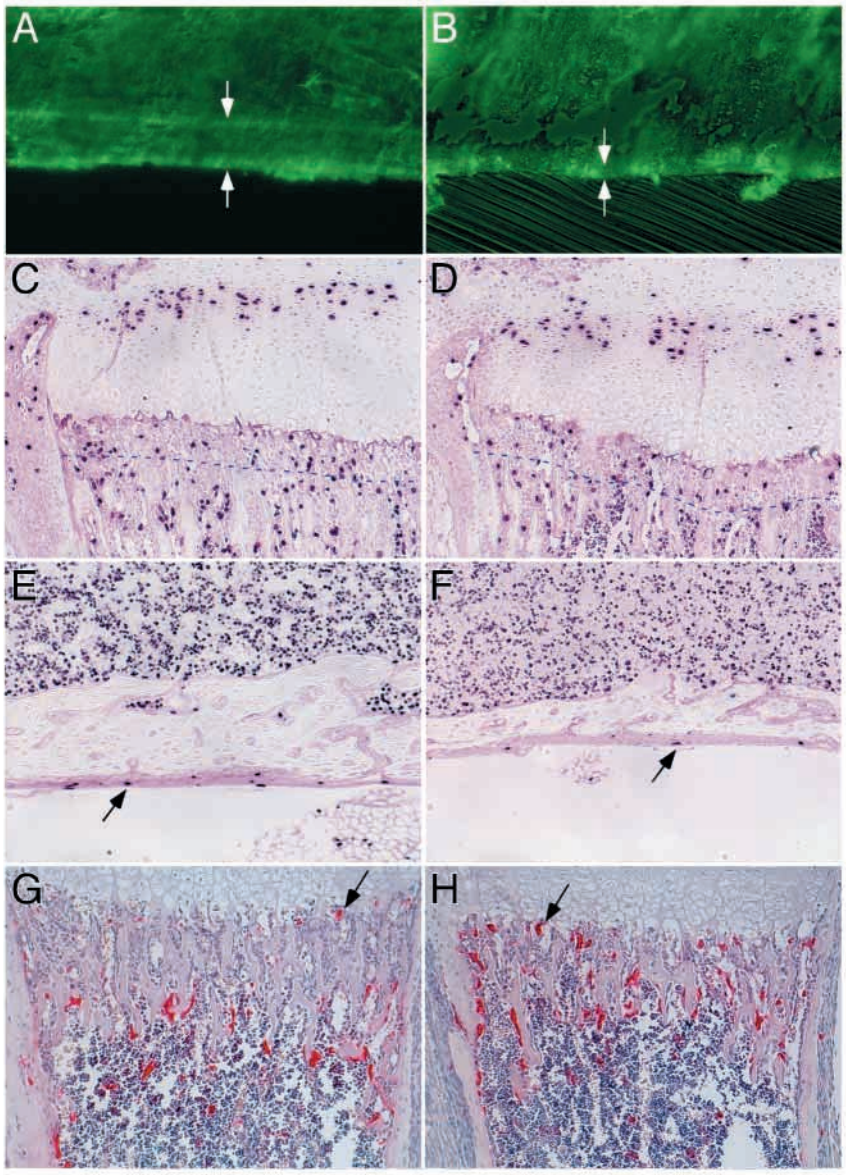

Fig. 7. Mineral apposition rate (MAR), osteoblast proliferation and osteoclast density in *Fgfr2*^{cko} mice. (A,B) MAR was assessed by calcein double labeling over a 9-day interval beginning at P8. (C,D) BrdU immunohistochemistry on sections of the femur from P15 mice showing the distal growth plate. The dashed lines parallel to the chondro-osseous junction demarcate the 100 μm region of the metaphysis that was counted (see Materials and Methods). The labeling index of the growth plate proliferating zone was similar for *Fgfr2*^{cko} mice and controls. In contrast, the osteoblast proliferation index in the primary spongiosa was reduced in *Fgfr2*^{cko} mice compared to controls (Table 3). (E,F) BrdU immunohistochemistry of the femoral diaphysis at P15. Note the proliferating osteoprogenitor cells located in the perichondrium (arrows). (G,H) TRAP staining of sections of the proximal femur at P4. Note that osteoclasts (stained in red) at the chondro-osseous junction appear larger and more numerous in *Fgfr2*^{cko} mice than in control littermates. Osteoclast densities were 1.29±0.29/0.01 mm^2 in control mice (n=6) and 1.82±0.37/0.01 mm^2 in *Fgfr2*^{cko} mice (n=6, P<0.001). (A,C,E,G) control mice. (B,D,F,H) *Fgfr2*^{cko} mice.

Fgfr2 signaling is required for osteoblast proliferation

During skeletal development, the osteoblast lineage undergoes continued proliferation to accommodate rapid bone growth during early postnatal development. The decreased total number of osteoblasts in osteogenic regions of *Fgfr2*^{cko} mice suggested that osteoblast proliferation could be dependent on FGFR2 signaling. BrdU labeling studies identified zones of proliferation in the perichrondrium and metaphysis, as well as in the mid diaphyseal periosteum. These osteogenic regions contained fewer proliferating osteoblasts in *Fgfr2*^{cko} mice compared with controls (Fig. 7C-F, Table 3).

Another possible reason for decreased cell number is increased cell death due to loss of *Fgfr2*. However, total numbers of apoptotic cells, analyzed by TUNEL labeling and caspase 3 immunohistochemistry, were similar in femur sections of *Fgfr2*^{cko} and control mice at both embryonic and postnatal stages (data not shown). These results suggested that *Fgfr2* was essential for proliferation but not survival of osteoblasts.

Reduced hypertrophic chondrocyte zone in *Fgfr2*^{cko} mice

Longitudinal bone growth is tightly coupled to proliferation and differentiation of chondrocytes in the growth plate. When either process is disrupted, longitudinal bone growth is affected. Since *Fgfr2*^{cko} mice also showed a dwarfism phenotype, the growth plate of *Fgfr2*^{cko} mice was examined. At all developmental stages examined, the growth plate of *Fgfr2*^{cko} mice showed an overall intact histomorphologic architecture (Fig. 6A,B). In *Fgfr2*^{cko} mice the length of the proliferation zone was similar to that of controls (Table 2) and the BrdU labeling index was not significantly changed (Fig. 7C,D). However, the length of the hypertrophic zone was greatly reduced during early postnatal development (Table 2). The length of the hypertrophic zone is controlled by the rate of proliferating chondrocyte differentiation and by osteoclast (chondroclast)-mediated degradation at the chondro-osseous junction (Gerber et al., 1999; Turner et al., 1994).

The Indian hedgehog (IHH) signaling pathway is an important regulator of chondrocyte proliferation and differentiation (Karsenty and Wagner, 2002; Ornitz and

Marie, 2002). The IHH receptor, *Patched*, is expressed by proliferating chondrocytes (St-Jacques et al., 1999) and its level of expression is a measure of the strength of the IHH signal (Chen and Struhl, 1996; Ingham, 1998). No significant difference was observed in *Patched* expression in *Fgfr2*^{cko} and control mice (data not shown), indicating that IHH activation in the growth plate was intact during skeletal development. These observations suggest that the primary cause of dwarfism and the reduced size of the hypertrophic zone are unlikely to be caused by defective chondrocyte differentiation.

Osteoclasts were examined by staining for TRAP activity. During embryogenesis (E16.5), no significant difference was found between control and *Fgfr2*^{cko} mice (data not shown). However during early postnatal development, although the distribution pattern of TRAP-positive cells was similar in *Fgfr2*^{cko} and control mice, the relative number of TRAP-positive cells in the chondro-osseous junction increased by 40% (n=6 mice, P<0.001) in *Fgfr2*^{cko} mice (Fig. 7G,H). Interestingly, osteoclasts were also more mature (larger) than in control mice.

DISCUSSION

Dermo1-CRE as a tool for targeting skeletal lineages

The CRE-LoxP system is an efficient method for tissue-specific gene modification during development. The success of this strategy depends on tissue-specific expression of CRE in the anlage of a targeted tissue at a time prior to the expression of the targeted gene. In this study a *Dermo1-cre* knockin mouse was used to probe the function of *Fgfr2* during skeletal development. *Dermo1*-CRE activity was present in condensed mesenchyme which gives rise to both the chondrocyte and osteoblast lineage. The specificity of *Dermo1*-CRE-mediated recombination was confirmed by lineage tracing analysis using the *R26R* mouse (Soriano, 1999). This analysis identified both osteoblasts and chondrocytes as lineage descendants of cells that express *Dermo1-cre*. The efficiency of CRE-mediated β-gal activation in these lineages approached 100 percent. In situ hybridization confirmed the efficiency of *Dermo1*-CRE-mediated gene deletion by demonstrating the absence of the floxed *Fgfr2* exons in skeletal tissue.

Fgfr2 is one of the earliest genes expressed in the mesenchymal condensation (Delezoide et al., 1998; Orr-Urtreger et al., 1991; Peters et al., 1992); probably before the very first expression of *Dermo1-cre* (Li et al., 1995). It is not known how long it takes for complete CRE-mediated gene inactivation after *cre* is first expressed and translated. It is therefore possible that FGFR2 protein is synthesized and retained in condensing mesenchymal cells, even after the *Fgfr2* gene is disrupted. The precise timing of *Fgfr2* inactivation could therefore lead to heterogeneity in the onset and possible severity of the skeletal phenotype. Because of this potential delay in *Fgfr2* inactivation, the complete function of FGFR2 in the mesenchymal condensation has not been clearly addressed by this study. However, based on the comparative expression patterns of *Dermo1-cre* and *Fgfr2*, we conclude that the skeletal phenotype in *Fgfr2*^{cko} mice is a direct cell autonomous consequence of loss of FGFR2 function in the osteoblast, following the formation of the mesenchymal condensation. Interestingly, introduction of a frame shift mutation into the c exon of *Fgfr2* resulted in a viable mouse with a similar degree of skeletal dwarfism and similar defects in skeletal morphology (Eswarakumar et al., 2002). However, in *Fgfr2IIIc*$^{-/-}$ mice a delay in ossification was observed whereas in *Fgfr2*^{cko} mice there was no delay in ossification. This may reflect differences in timing of *Fgfr2* inactivation.

Regulation of osteoblast development

Recent studies have established the transcription factor *Cbfa1* as a determinant of osteoblast differentiation. *Cbfa1* is the earliest and most specific gene expressed during osteoblast differentiation. In *Cbfa1*-deficient mice, the osteoblast differentiation process is completely blocked (Komori et al., 1997; Otto et al., 1997). CBFA1 controls the expression of genes that encode various bone matrix proteins. The similar expression of *Cbfa1* and other osteoblast-specific genes in both *Fgfr2*^{cko} and control mice indicated that *Fgfr2* is not necessary for the early stages of osteoblast differentiation. However, osteoblast differentiation is normally accompanied by profound morphological and functional changes. Osteoprogenitor cells, which appear morphologically like fibroblasts, are relatively small and have a compact cytoplasm. Although osteoprogenitor cells produce bone matrix proteins, their main function is to maintain the progenitor pool through proliferation. In contrast, mature osteoblasts are plump cuboidal cells with ample cytoplasm. Electron microscopy studies reveal that the cytoplasm of mature osteoblasts contains large amounts of rough endoplasmic reticulum and an extensive Golgi apparatus, consistent with their function in synthesizing large amounts of bone matrix proteins. The presence of atrophic cytoplasm in osteoblasts of *Fgfr2*^{cko} mice and the dramatically decreased MAR strongly indicates that their protein synthesis capacity was reduced. *Fgfr2* was expressed by osteoprogenitor cells in perichondrial and periosteal tissues (Fig. 1H,K) and by mature osteoblasts in the metaphysis, and in diaphyseal lacunae (Fig. 1K). Notably, osteoblasts in diaphyseal lacunae were post mitotic (Fig. 7E). The *Fgfr2* expression pattern and the osteogenic phenotype in *Fgfr2*^{cko} mice suggests that FGFR2 signaling regulates proliferation of osteoprogenitor cells and the anabolic function of mature osteoblasts. Consistent with this observation, the effect of implanting FGF2 beads over the coronal suture in mice suggested that the primary function of FGFR2 is to regulate osteoblast proliferation in suture mesenchyme (Iseki et al., 1999).

It has been shown that FGFR1 signaling can directly regulate *Cbfa1* expression in osteoblasts (Zhou et al., 2000). In this study, loss of *Fgfr2* did not affect *Cbfa1* expression, suggesting that FGFR2 signaling may function in a *Cbfa1*-independent manner. Whether *Cbfa1* is directly involved in osteoblast proliferation is not clear. Interestingly, *low-density lipoprotein receptor-related protein (Lrp)-5*-deficient mice have been shown to have a *Cbfa1*-independent decrease in osteoblast proliferation and bone formation (Kato et al., 2002). Since LRP5 mediates WNT signaling, these data, together with this study, suggest that proliferation of the osteoblast lineage is regulated by multiple signaling pathways that do not require CBFA1 as a downstream effector. Moreover, the morphological characteristics of mature osteoblasts are similar to other cell-types engaged in the synthesis and secretion of large amounts of proteins. This also suggests non-lineage-specific regulation

of metabolic function because, unlike the complete lack of bone formation in *Cbfa1*-deficient mice, the diminished bone formation in *Fgfr2^{cko}* mice suggests that FGFR2 signaling is complementary to that of CBFA1 during skeletal development. Indeed, we have identified a transcriptional activation domain in CBFA1 that is markedly enhanced in response to FGFR2 activation (D.A.T. and D.M.O., unpublished).

Metaphyseal osteogenesis as a determinant of longitudinal bone growth

Skeletal dwarfism is often associated with decreased chondrocyte proliferation. In ACH, the hypertrophic zone is shortened as a result of reduced chondrocyte proliferation and differentiation (Naski et al., 1998; Ornitz and Marie, 2002). In contrast, *Fgfr2^{cko}* mice have decreased bone length without apparent defects in chondrocyte proliferation. However, similar to *Fgfr2IIIc$^{-/-}$* mice (Eswarakumar et al., 2002), *Fgfr2^{cko}* mice also exhibit a shortened hypertrophic zone. Interestingly, the decreased length of the hypertrophic zone in *Fgfr2^{cko}* mice was accompanied by an increase in the number of mature osteoclasts in the chondro-osseous junction. Increased osteoclast activity could account for the decrease in hypertrophic zone length by increasing the rate of removal of calcified hypertrophic chondrocyte matrix. Furthermore, in contrast to ACH, in which bone formation in the diaphysis is not affected and diaphyseal cortical bone has normal thickness (Rimoin et al., 1970), *Fgfr2^{cko}* mice showed a dramatic reduction in diaphyseal thickness. These data suggest that the pathogenesis of the dwarfism in *Fgfr2^{cko}* mice is significantly different from that of ACH and that metaphyseal osteogenesis, which is severely affected in *Fgfr2^{cko}* mice, is an important regulator of longitudinal bone growth.

Fgfr2^{cko} mice exhibit decreased bone density throughout their life (examined up to 58 weeks). The finding that FGFR2 is required by the osteoblast to regulate mineral deposition suggests that FGF signaling may be important for the maintenance of bone density.

We thank Ling Li, Heather Walker and Craig Smith for their excellent technical help, X. Hua for microinjection, the Washington University Siteman Cancer Center Embryonic Stem Cell core facility for ES cell culture and the MBP histology core facility. This work was supported by NIH grants HD39952, CA60673, DK52446 (D.A.T.) and DK52574 (microinjection) and a generous contribution from the Virginia Friedhofer Charitable Trust.

REFERENCES

Anderson, J., Burns, H. D., Enriquez-Harris, P., Wilkie, A. O. M. and Heath, J. K. (1998). Apert syndrome mutations in fibroblast growth factor receptor 2 exhibit increased affinity for FGF ligand. *Hum. Mol. Genet.* **7**, 1475-1483.

Bustin, S. A. (2000). Absolute quantification of mRNA using real-time reverse transcription polymerase chain reaction assays. *J. Mol. Endocrinol.* **25**, 169-193.

Caplan, A. I. and Pechak, D. G. (1987). The cellular and molecular embryology of bone formation. In *Bone and Mineral Research*, vol. 5 (ed. W. A. Peck), pp. 117-183. New York: Elsevier Science Publishers.

Chen, L., Adar, R., Yang, X., Monsonego, E. O., Li, C., Hauschka, P. V., Yayon, A. and Deng, C. X. (1999). Gly369Cys mutation in mouse FGFR3 causes achondroplasia by affecting both chondrogenesis and osteogenesis. *J. Clin. Invest.* **104**, 1517-1525.

Chen, L., Li, C., Qiao, W., Xu, X. and Deng, C. (2001). A Ser(365)–>Cys mutation of fibroblast growth factor receptor 3 in mouse downregulates Ihh/PTHrP signals and causes severe achondroplasia. *Hum. Mol. Genet.* **10**, 457-465.

Chen, Y. and Struhl, G. (1996). Dual roles for patched in sequestering and transducing Hedgehog. *Cell* **87**, 553-563.

Chikazu, D., Katagiri, M., Ogasawara, T., Ogata, N., Shimoaka, T., Takato, T., Nakamura, K. and Kawaguchi, H. (2001). Regulation of osteoclast differentiation by fibroblast growth factor 2: stimulation of receptor activator of nuclear factor kappaB ligand/osteoclast differentiation factor expression in osteoblasts and inhibition of macrophage colony-stimulating factor function in osteoclast precursors. *J. Bone Miner. Res.* **16**, 2074-2081.

Cohen, M. M. J. (2000). Apert Syndrome. In *Craniosynostosis, Diagnosis, Evaluation, and Management* (ed. M. M. J. Cohen and R. E. MacLean), pp. 316-353. New York: Oxford University Press.

Colvin, J. S., Bohne, B. A., Harding, G. W., McEwen, D. G. and Ornitz, D. M. (1996). Skeletal overgrowth and deafness in mice lacking fibroblast growth factor receptor 3. *Nat. Genet.* **12**, 390-397.

De Moerlooze, L., Spencer-Dene, B., Revest, J., Hajihosseini, M., Rosewell, I. and Dickson, C. (2000). An important role for the IIIb isoform of fibroblast growth factor receptor 2 (FGFR2) in mesenchymal-epithelial signalling during mouse organogenesis. *Development* **127**, 483-492.

Delezoide, A. L., Benoistlasselin, C., Legeaimallet, L., Lemerrer, M., Munnich, A., Vekemans, M. and Bonaventure, J. (1998). Spatio-temporal expression of Fgfr 1, 2 and 3 genes during human embryo-fetal ossification. *Mech. Dev.* **77**, 19-30.

Dymecki, S. M. (1996). A modular set of Flp, FRT and lacZ fusion vectors for manipulating genes by site-specific recombination. *Gene* **171**, 197-201.

Eswarakumar, V. P., Monsonego-Ornan, E., Pines, M., Antonopoulou, I., Morriss-Kay, G. M. and Lonai, P. (2002). The IIIc alternative of Fgfr2 is a positive regulator of bone formation. *Development* **129**, 3783-3793.

Gerber, H. P., Vu, T. H., Ryan, A. M., Kowalski, J., Werb, Z. and Ferrara, N. (1999). VEGF couples hypertrophic cartilage remodeling, ossification and angiogenesis during endochondral bone formation. *Nat. Med.* **5**, 623-628.

Ingham, P. W. (1998). Transducing hedgehog: the story so far. *EMBO J.* **17**, 3505-3511.

Iseki, S., Wilkie, A. O. and Morriss-Kay, G. M. (1999). Fgfr1 and Fgfr2 have distinct differentiation- and proliferation-related roles in the developing mouse skull vault. *Development* **126**, 5611-5620.

Iwata, T., Li, C. L., Deng, C. X. and Francomano, C. A. (2001). Highly activated Fgfr3 with the K644M mutation causes prolonged survival in severe dwarf mice. *Hum. Mol. Genet.* **10**, 1255-1264.

Jabs, E. W., Li, X., Scott, A. F., Meyers, G., Chen, W., Eccles, M., Mao, J., Charnas, L. R., Jackson, C. E. and Jaye, M. (1994). Jackson-Weiss and Crouzon syndromes are allelic with mutations in fibroblast growth factor receptor 2. *Nat. Genet.* **8**, 275-279.

Karsenty, G. and Wagner, E. F. (2002). Reaching a genetic and molecular understanding of skeletal development. *Dev. Cell* **2**, 389-406.

Kato, M., Patel, M. S., Levasseur, R., Lobov, I., Chang, B. H., Glass, D. A., 2nd, Hartmann, C., Li, L., Hwang, T. H., Brayton, C. F. et al. (2002). Cbfa1-independent decrease in osteoblast proliferation, osteopenia, and persistent embryonic eye vascularization in mice deficient in Lrp5, a Wnt coreceptor. *J. Cell Biol.* **157**, 303-314.

Komori, T., Yagi, H., Nomura, S., Yamaguchi, A., Sasaki, K., Deguchi, K., Shimizu, Y., Bronson, R. T., Gao, Y. H., Inada, M. et al. (1997). Targeted disruption of Cbfa1 results in a complete lack of bone formation owing to maturational arrest of osteoblasts. *Cell* **89**, 755-764.

Lewandoski, M., Meyers, E. N. and Martin, G. R. (1997a). Analysis of Fgf8 gene function in vertebrate development. *Cold Spring Harb. Symp. Quant. Biol.* **62**, 159-168.

Lewandoski, M., Wassarman, K. M. and Martin, G. R. (1997b). Zp3-cre, a transgenic mouse line for the activation or inactivation of loxP-flanked target genes specifically in the female germ line. *Curr. Biol.* **7**, 148-151.

Li, C., Chen, L., Iwata, T., Kitagawa, M., Fu, X. Y. and Deng, C. X. (1999). A Lys644Glu substitution in fibroblast growth factor receptor 3 (FGFR3) causes dwarfism in mice by activation of STATs and ink4 cell cycle inhibitors. *Hum. Mol. Genet.* **8**, 35-44.

Li, L., Cserjesi, P. and Olson, E. N. (1995). Dermo-1: a novel twist-related bHLH protein expressed in the developing dermis. *Dev. Biol.* **172**, 280-292.

Liu, Z., Xu, J., Colvin, J. S. and Ornitz, D. M. (2002). Coordination of chondrogenesis and osteogenesis by fibroblast growth factor 18. *Genes Dev.* **16**, 859-869.

McEwen, D. G. and Ornitz, D. M. (1997). Determination of fibroblast growth

factor receptor expression in mouse, rat and human samples using a single primer pair. *Biotechniques* **22**, 1068-1070.

Metsaranta, M., Toman, D., de Crombrugghe, B. and Vuorio, E. (1991). Specific hybridization probes for mouse type I, II, III and IX collagen mRNAs. *Biochim. Biophys. Acta* **1089**, 241-243.

Miki, T., Bottaro, D. P., Fleming, T. P., Smith, C. L., Burgess, W. H., Chan, A. M. and Aaronson, S. A. (1992). Determination of ligand-binding specificity by alternative splicing: two distinct growth factor receptors encoded by a single gene. *Proc. Natl. Acad. Sci. USA* **89**, 246-250.

Min, H., Danilenko, D. M., Scully, S. A., Bolon, B., Ring, B. D., Tarpley, J. E., DeRose, M. and Simonet, W. S. (1998). Fgf-10 is required for both limb and lung development and exhibits striking functional similarity to *Drosophila* branchless. *Genes Dev.* **12**, 3156-3161.

Naski, M. C., Colvin, J. S., Coffin, J. D. and Ornitz, D. M. (1998). Repression of hedgehog signaling and BMP4 expression in growth plate cartilage by fibroblast growth factor receptor 3. *Development* **125**, 4977-4988.

Naski, M. C. and Ornitz, D. M. (1998). FGF signaling in skeletal development. *Front. Biosci.* **3**, D781-D794.

Newberry, E. P., Boudreaux, J. M. and Towler, D. A. (1996). The rat osteocalcin fibroblast growth factor (FGF)-responsive element: an okadaic acid-sensitive, FGF-selective transcriptional response motif. *Mol. Endocrinol.* **10**, 1029-1040.

Newberry, E. P., Willis, D., Latifi, T., Boudreaux, J. M. and Towler, D. A. (1997). Fibroblast growth factor receptor signaling activates the human interstitial collagenase promoter via the bipartite Ets-AP1 element. *Mol. Endocrinol.* **11**, 1129-1144.

Ornitz, D. M. and Itoh, N. (2001). Fibroblast growth factors. *Genome Biol.* **2**, REVIEWS3005.

Ornitz, D. M. and Marie, P. J. (2002). FGF signaling pathways in endochondral and intramembranous bone development and human genetic disease. *Genes Dev.* **16**, 1446-1465.

Ornitz, D. M., Xu, J., Colvin, J. S., McEwen, D. G., MacArthur, C. A., Coulier, F., Gao, G. and Goldfarb, M. (1996). Receptor specificity of the fibroblast growth factor family. *J. Biol. Chem.* **271**, 15292-15297.

Orr-Urtreger, A., Bedford, M. T., Burakova, T., Arman, E., Zimmer, Y., Yayon, A., Givol, D. and Lonai, P. (1993). Developmental localization of the splicing alternatives of fibroblast growth factor receptor-2 (FGFR2). *Dev. Biol.* **158**, 475-486.

Orr-Urtreger, A., Givol, D., Yayon, A., Yarden, Y. and Lonai, P. (1991). Developmental expression of two murine fibroblast growth factor receptors, *flg* and *bek*. *Development* **113**, 1419-1434.

Otto, F., Thornell, A. P., Crompton, T., Denzel, A., Gilmour, K. C., Rosewell, I. R., Stamp, G. W., Beddington, R. S., Mundlos, S., Olsen, B. R. et al. (1997). Cbfa1, a candidate gene for cleidocranial dysplasia syndrome, is essential for osteoblast differentiation and bone development. *Cell* **89**, 765-771.

Peters, K. G., Werner, S., Chen, G. and Williams, L. T. (1992). Two FGF receptor genes are differentially expressed in epithelial and mesenchymal tissues during limb formation and organogenesis in the mouse. *Development* **114**, 233-243.

Rimoin, D. L., Hughes, G. N., Kaufman, R. L., Rosenthal, R. E., McAlister, W. H. and Silberberg, R. (1970). Endochondral ossification in achondroplastic dwarfism. *N. Engl. J. Med.* **283**, 728-735.

Rutland, P., Pulleyn, L. J., Reardon, W., Baraitser, M., Hayward, R., Jones, B., Malcolm, S., Winter, R. M., Oldridge, M., Slaney, S. F. et al. (1995). Identical mutations in the FGFR2 gene cause both Pfeiffer and Crouzon syndrome phenotypes. *Nat. Genet.* **9**, 173-176.

Segev, O., Chumakov, I., Nevo, Z., Givol, D., Madar-Shapiro, L., Sheinin, Y., Weinreb, M. and Yayon, A. (2000). Restrained chondrocyte proliferation and maturation with abnormal growth plate vascularization and ossification in human FGFR-3(G380R) transgenic mice. *Hum. Mol. Genet.* **9**, 249-258.

Sekine, K., Ohuchi, H., Fujiwara, M., Yamasaki, M., Yoshizawa, T., Sato, T., Yagishita, N., Matsui, D., Koga, Y., Itoh, N. et al. (1999). Fgf10 is essential for limb and lung formation. *Nat. Genet.* **21**, 138-141.

Soriano, P. (1999). Generalized lacZ expression with the ROSA26 Cre reporter strain. *Nat. Genet.* **21**, 70-71.

St-Jacques, B., Hammerschmidt, M. and McMahon, A. P. (1999). Indian hedgehog signaling regulates proliferation and differentiation of chondrocytes and is essential for bone formation. *Genes Dev.* **13**, 2072-2086.

Turner, R. T., Evans, G. L. and Wakley, G. K. (1994). Reduced chondroclast differentiation results in increased cancellous bone volume in estrogen-treated growing rats. *Endocrinology* **134**, 461-466.

Tybulewicz, V. L. J., Crawford, C. E., Jackson, P. K., Bronson, R. T. and Mulligan, R. C. (1991). Neonatal lethality and lymphopenia in mice with a homozygous disruption of the *c-abl* proto-oncogene. *Cell* **65**, 1153-1163.

Wang, Y. C., Spatz, M. K., Kannan, K., Hayk, H., Avivi, A., Gorivodsky, M., Pines, M., Yayon, A., Lonai, P. and Givol, D. (1999). A mouse model for achondroplasia produced by targeting fibroblast growth factor receptor 3. *Proc. Natl. Acad. Sci. USA* **96**, 4455-4460.

Wilkie, A. O. M. (1997). Craniosynostosis- genes and mechanisms. *Hum. Mol. Genet.* **6**, 1647-1656.

Willis, D. M., Loewy, A. P., Charlton-Kachigian, N., Shao, J. S., Ornitz, D. M. and Towler, D. A. (2002). Regulation of osteocalcin gene expression by a novel ku antigen transcription factor complex. *J. Biol. Chem.* **277**, 37280-37291.

Xu, X., Weinstein, M., Li, C., Naski, M., Cohen, R. I., Ornitz, D. M., Leder, P. and Deng, C. (1998). Fibroblast growth factor receptor 2 (FGFR2)-mediated regulation loop between FGF8 and FGF10 is essential for limb induction. *Development* **125**, 753-765.

Yu, K., Herr, A. B., Waksman, G. and Ornitz, D. M. (2000). Loss of fibroblast growth factor receptor 2 ligand-binding specificity in Apert syndrome. *Proc. Natl. Acad. Sci. USA* **97**, 14536-14541.

Yu, K. and Ornitz, D. M. (2001). Uncoupling fibroblast growth factor receptor 2 ligand binding specificity leads to Apert syndrome-like phenotypes. *Proc. Natl. Acad. Sci. USA* **98**, 3641-3643.

Zhou, Y. X., Xu, X., Chen, L., Li, C., Brodie, S. G. and Deng, C. X. (2000). A Pro250Arg substitution in mouse Fgfr1 causes increased expression of Cbfa1 and premature fusion of calvarial sutures. *Hum. Mol. Genet.* **9**, 2001-2008.